

# Velocity measurements of turbulence collapse in a linearly stratified jet

D. R. Webster, Y. Liu

394

**Abstract** The behavior of a horizontal turbulent round jet in a linearly density-stratified fluid is studied and compared to the unstratified case using digital particle-tracking velocimetry (DPTV). Close to the nozzle, the stratified jet grows axisymmetrically at the same rate as an unstratified jet. At a critical distance downstream, the vertical growth is suppressed, while the lateral spreading increases. The self-similar nature of unstratified round jets is not preserved in the stratified case. The velocity field and turbulent stresses are affected by the stratification closer to the jet nozzle than is expected from the flow visualization observations. In particular, the vertical normal stress and shear stress are significantly reduced compared to the unstratified case.

## 1 Introduction

Turbulent jets into a density-stratified fluid occur in a wide range of engineering and geophysical contexts. A primary example is the discharge of wastewater into a density-stratified lake or ocean layer. Shear layer turbulence in stable density-stratified environments is unique because the buoyant “production” term in the turbulent kinetic energy budget acts to destroy turbulent kinetic energy, thus dampening turbulent transport especially in the vertical direction. Active turbulence collapses and eventually becomes “fossilized”, a state characterized by 2D internal waves and/or quasi-2D turbulence (Gibson 1980).

This study focuses on a horizontal, neutrally buoyant, turbulent jet discharging into linearly density-stratified ambient fluid. The behavior of a round jet into an unstratified environment has been studied extensively and is well understood (e.g., Fischer et al. 1979). While the density-stratified case has been studied less, several important observations have been made based on the flow visualization of Gibson (1987 and 1990) and Roberts and Matthews (1987). (In addition, Roberts and Matthews (1984) examined horizontal jets in a two-layer system with a homogeneous upper layer and a linearly stratified lower layer.) Close to the nozzle, the jet turbulence is

energetic and the growth rate is unaffected by the stratification. After turbulence collapse, the vertical growth rate is greatly reduced, thus trapping the jet fluid in a thin horizontal layer. To date no quantitative velocity field measurements have been published, and the turbulent jet characteristics have been inferred from flow visualization observations.

Scaling arguments for a fully turbulent jet suggest that the flow is characterized by the flux of volume,  $Q = \pi UD^2/4$ , and momentum,  $M = \pi U^2 D^2/4$ . Two relevant length scales are defined to characterize the jet flow in a stratified layer:  $l_Q = Q/M^{1/2}$  and  $l_N = M^{1/4}/N^{1/2}$  where  $N = \{-g(d\rho/dz)/\rho\}^{1/2}$  is the buoyancy frequency. Jet characteristics are independent of the volume flow rate beyond  $7l_Q$  (at  $x/D = 6.2$  for the round jet discussed here). Thus, the effect of stratification will be noted by a deviation compared to the unstratified jet profile at a particular  $x/l_N$  location. Roberts and Matthews (1987) reported that the transition occurs around  $x_m/l_N = 2.8$  with a jet height of  $w_l/l_N = 0.95$  for the range of parameters examined. Extending the dimensional argument to the dilution of dye released in the jet, Roberts et al. (2001) confirmed that the normalized dilution deviates from the unstratified behavior around  $x/l_N = 4$ , i.e., slightly further from the nozzle than inferred from the flow visualization.

Gibson (1987) states that fossilization begins when buoyant forces first balance the inertial forces. He argued that this occurs when the Ozmidov length scale reaches approximately 1.5 times the vertical jet width,  $L_R \approx (1.5 \pm 0.5)w$ . In Gibson’s active-fossil region, the turbulence scale decreases until the inertial forces of the turbulence are comparable to the viscous forces. Gibson (1987) also estimated the distance for ultimate collapse (complete fossilization) to occur when  $11L_K \approx L_R$ , where  $L_K$  is the Kolmogorov scale. Alternatively, Ivey and Imberger (1991) defined an overturn Froude number,  $Fr_T = u_{rms}/NL_C = (L_R/L_C)^{2/3}$ , which is the ratio of the Ozmidov scale to the most energetic overturn length scale, to characterize the transition from active turbulence.

Significant insight has been gained in recent years by examining the idealized case of homogeneous turbulence subject to linear shear and stratification via experiments (Rohr et al. 1988; Piccirillo and Van Atta 1997) and direct numerical simulation (Holt et al. 1992; Jacobitz et al. 1997; Shih et al. 2000). Rohr et al. (1988) found excellent agreement with linear inviscid stability analysis; specifically that turbulence is suppressed at gradient Richardson number,  $Ri = N^2/(\partial U/\partial z)^2$ , equal to  $0.25 \pm 0.05$ . Holt et al. (1992) found that the stationary Richardson number

Received: 11 September 2000/Accepted: 28 March 2001

D. R. Webster (✉), Y. Liu  
School of Civil and Environmental Engineering  
Georgia Institute of Technology  
Atlanta, GA 30332, USA

is a function of  $Re$  due to variation in dissipation rate. More recently, Shih et al. (2000) showed that at large  $Re$  the dimensionless shear number  $S^* = Sq^2/\varepsilon$  approaches a constant value around 11 independent of the initial conditions.

While these studies provide insight into the basic interaction of turbulence with stable stratification, more complex shear flows have received less attention. In addition to the jet flow studies mentioned above, Boyer et al. (1989) and Xu et al. (1995) have studied the wake of a cylinder moving through a density-stratified fluid. For large internal Froude number,  $Fi = U/ND > 2$ , the wake grows to a maximum size and then the growth collapses. The final patch thickness was approximately  $1.8D$  in each case. In the wake of the cylinder, power spectra show a  $k^{-3}$  regime growing at the expense of the  $k^{-5/3}$  regime, which indicates turbulent collapse and the development of 2D turbulence. At low Reynolds number, List (1971) provided an analytical solution for a horizontal jet in a linearly stratified layer. Interestingly, rotors form above and below the jet as a result of the density stratification. Also at low Reynolds number, Voropayev and Afanasyev (1991) experimentally observed that stratification had a minimal effect on the jet velocity profiles. This result is in contrast to the turbulent results presented here.

The objective of this paper is to report the turbulent velocity field measured via digital particle-tracking velocimetry (DPTV) for a horizontal turbulent jet into density-stratified ambient. DPTV is part of a broad class of non-intrusive techniques that measure the fluid velocity by observing the displacement of tracer particles over a short time delay. Subsequent analysis of a series of velocity fields yields the mean flow and turbulent statistics of the collapsing jet. The ultimate goal is to better understand the turbulence collapse.

## 2

### Experiment description

Experiments were conducted in a 0.6-m-deep, 0.9-m-wide, and 1-m-long test tank as shown in Fig. 1. The front and end walls of the tank were glass, while the other walls and floor were aluminum painted black. In our experiments, the jet collapsed roughly 0.3 m from the nozzle with a height of approximately 0.1 m, thus the boundaries are distant from the jet flow.

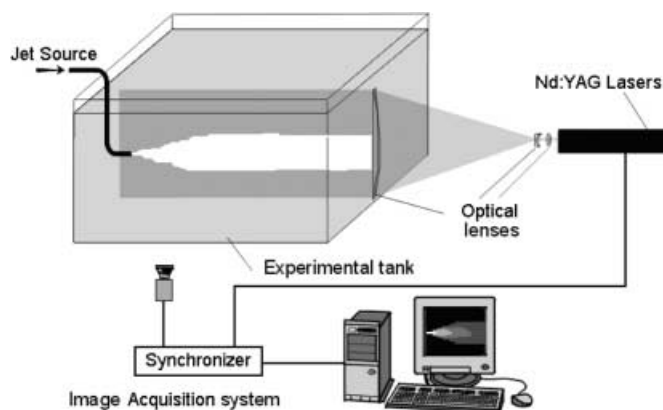


Fig. 1. Sketch of flow facility

## 2.1

### Density stratification and index of refraction matching

The experimental test tank was filled by following the “slip-under” method of Fortuin (1960). Tank A was filled with the more dense liquid (salt solution) and tank B was filled with the less dense liquid (ethanol solution). The test tank was filled by continuously pumping dense solution from tank A to tank B at a flow rate of  $Q_A$  and from tank B into the test tank at a flow rate of  $Q_B (= 2Q_A)$ . The solution in tank B was continuously mixed; thus, the fluid density in tank B increased linearly with time.

A diffuser is located near the floor at the rear of the test tank with an inner diameter of 25 mm and 20 3.2-mm-diameter ports spaced 25 mm apart. Fluid entering the test tank slid under and lifted the previous lighter layer, eventually creating a continuously stratified volume. Filling the tank slowly ( $Q_B = 6$  l/min) minimized mixing and disturbance between the layers. After filling, the volume was left alone for 2 h to allow diffusion to smooth any sharp discontinuities in the stratification. To determine the density gradient, a calibrated Troemner specific-gravity scale measured the density of samples from six depths in the test tank. A linear fit to the profile yielded the density gradient and buoyancy frequency. The buoyancy frequency was  $N = 0.5$  s<sup>-1</sup> for the stratified case presented here.

The refractive index varies with the density of the fluid, thus would generally change significantly with depth in the test tank. Distortions due to variation in the index of refraction of the fluid are a serious detriment to accurate velocity measurements. To avoid distortion problems, we followed the refractive-index-matching technique described in Hannoun et al. (1988) and Daviero et al. (2001). In the two-tank filling system described previously, the heavy salt solution and light ethanol solution both were prepared with a refractive index equal to 1.3346. A mixture of ethanol and salt solution that have a matched refractive index produces a new solution with a refractive index in close agreement with the original value. Therefore, the test tank was filled with a nearly uniform refractive index fluid whose density linearly varied in the vertical direction. The refractive index of the extracted samples was measured to confirm uniformity; in this case samples from six depths each yielded a refractive index of  $1.3346 \pm 0.00005$ .

## 2.2

### Jet flow

The jet flow discharged from a round brass nozzle with a 3.175-mm inner diameter. The effluent density matched the ambient density at the nozzle height and the index of refraction was matched with the ambient fluid. Velocity fields were measured for a turbulent jet with Reynolds number 4400 into stratified and unstratified environments.

## 2.3

### Velocity measurements

Velocity measurements were performed using DPTV. The technique is based on the idea that the instantaneous fluid velocity can be evaluated by recording the displacement of small tracer particles over short time intervals. Laser light

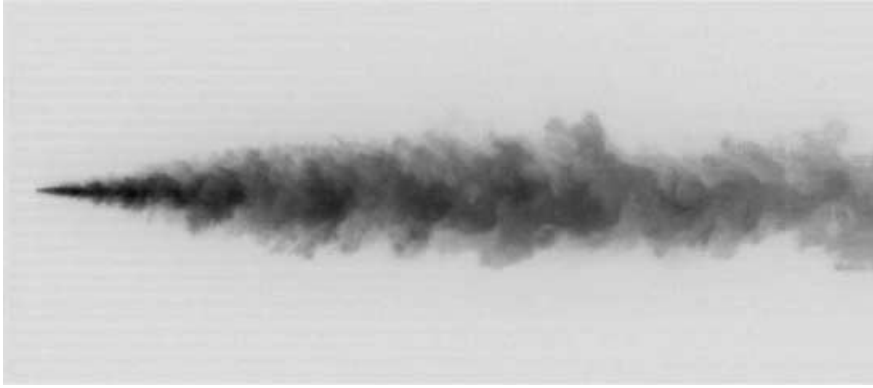


Fig. 2. Flow visualization for the stratified jet

scattered from the tracer particles is recorded with a CCD camera. Particle locations in consecutive images are compared to determine the local particle displacement.

Titanium dioxide ( $\text{TiO}_2$ ) particles, which have a specific gravity of 3.5 and nominal diameter less than  $5 \mu\text{m}$ , were added to both the ambient fluid and the jet effluent. The particles were added to the solutions in tanks A and B before filling the test tank and thus were uniformly distributed throughout the stratified layer. The inertial time constant of the particles was approximately  $2 \mu\text{s}$  and the settling velocity was  $12 \mu\text{m/s}$ , both of which are negligibly small for this flow.

The flow was illuminated with two pulsed Nd:YAG lasers (130 mJ at 532 nm, 6 ns duration). The time separation between the two pulses was 10 ms. The emitted laser beam passed through a combination of lenses designed to focus and expand the light into a thin sheet. The lenses were a 1000-mm focal length spherical lens, which focused the sheet to approximately 1 mm thickness in the photographic region, and a  $-12.7$ -mm focal-length cylindrical plano-concave lens, which expanded the beam into a vertical sheet. A large 450-mm focal-length cylindrical plano-convex lens was placed at the glass wall of the tank to collimate the expanding laser sheet into a parallel-edge sheet roughly 120 mm in height.

A Kodak Megaplug ES1.0 CCD camera was used to capture the images. The active sensor array consisted of  $1008$  (horizontal)  $\times$   $1018$  (vertical) pixels. A 60-mm Nikon aberration-free lens was employed on the camera. One thousand image pairs were collected at 10 Hz and stored on a hard-drive array in real time using the Video Savant RTD software. Hence, the data collection lasted 100 s and was complete before the finite tank volume was problematic. This was confirmed by observing that velocity time records at several points were statistically stationary and by flow visualization observations of the jet flow interaction with the endwall.

The DPTV analysis technique followed that of Cowen and Monismith (1997). To improve the efficiency of the particle pair search, the velocity field was first calculated via a standard cross-correlation DPIV algorithm between  $32 \times 32$ -pixel non-overlapping sub-windows. Individual particles were then identified as regions where the brightness was 50 gray levels above the background. The center of each particle was determined with a Gaussian sub-pixel fit estimation. Cross-correlation between  $9 \times$

$9$ -pixel interrogation windows centered on the DPIV prediction refines the displacement estimate. If one and only one particle was found in a  $3 \times 3$  sub-window centered on the refined estimate, then it was considered the displaced particle. The displacement distance was calculated as the difference between the particle centers.

In order to calculate the turbulent statistics, individual vectors were grouped into  $16 \times 16$ -pixel bins. Every vector located in the bin was included in the statistics, and the results were located at the center of the bin.

### 3 Results and discussion

Flow visualization images – a sample laser-induced fluorescence (LIF) image is shown in Fig. 2 – confirm the qualitative behavior of a jet into a stratified layer described by previous investigators. Close to the nozzle the jet expands radially in the same manner as the unstratified jet. At a critical distance from the nozzle the vertical expansion is suppressed, while the horizontal spreading is enhanced (for a photograph of horizontal spreading, see Fig. 4 in Roberts and Matthews 1987). Estimates from the flow visualization images indicate that  $x_m/l_N = 2.9$  and  $w_L/l_N = 0.93$ , which is in good agreement with Roberts and Matthews (1987).

Figure 3 shows a sample instantaneous velocity field measured for the stratified jet. Roughly 1500 velocity vectors were found in each instantaneous field. The measurement region corresponds to  $1.9 < x/l_N < 5.9$  in order to fully span the expected collapse location,  $x/l_N = 2.9$ .

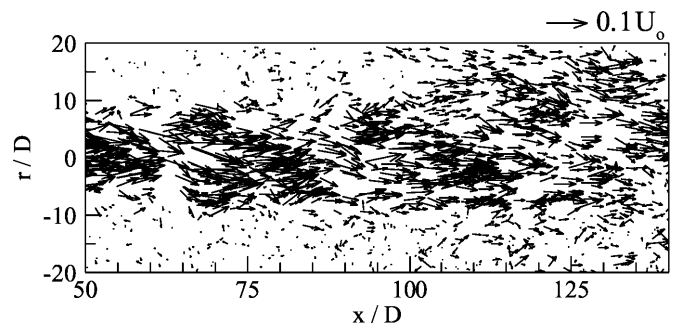


Fig. 3. Instantaneous velocity field for the stratified jet ( $x/l_N = 1.9 - 5.2$ )

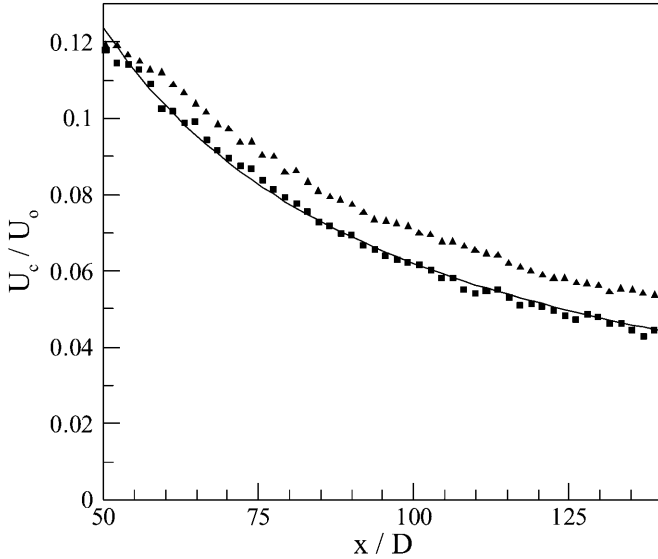


Fig. 4. Mean centerline velocity for the unstratified (■) and stratified (▲) jets. The curve is the semi-empirical expression  $U_c/U_o = 6.2D/x$

Figures 4–6 show the decay of the mean velocity, horizontal normal stress, and vertical normal stress along the centerline for both the stratified and unstratified jets. In each case, the semi-empirical curve for the unstratified jet is also shown (Fischer et al. 1979). For the mean velocity (Fig. 4), the unstratified jet measurements agree well with the semi-empirical curve. In the stratified case, the centerline velocity decays at a slower rate. This is consistent with the notion that attenuated vertical fluctuations (and shear stress) have a relatively diminished ability to mix momentum across the shear layer. The deviation of the centerline velocity from that of an unstratified jet occurs much closer to the nozzle than the collapse location  $x/l_N = 2.9$  ( $x/D = 80$ ) inferred from the flow visualization.

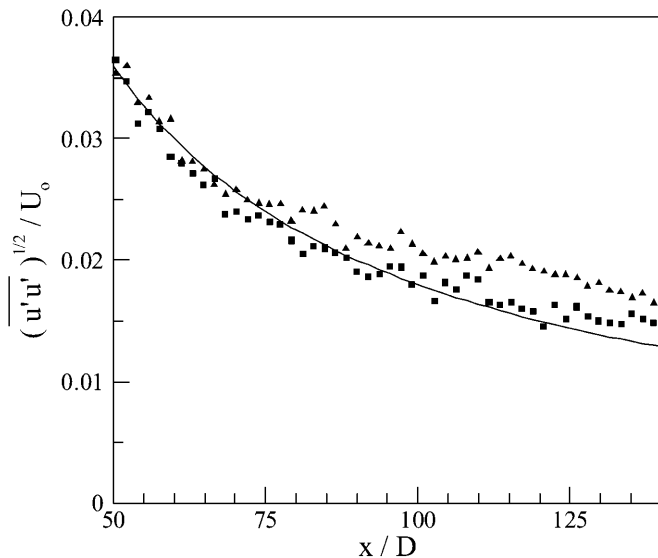


Fig. 5. Horizontal normal stress for the unstratified (■) and stratified (▲) jets. The curve is the semi-empirical expression  $(\overline{u'u'})^{1/2}/U_o = 1.8D/x$

The transition location for the horizontal normal stress (Fig. 5) agrees well with the flow visualization observations. Again, the unstratified data agrees well with the semi-empirical curve. For ( $x/D < 80$ ), the horizontal normal stress for the stratified jet agrees with the unstratified curve. Farther downstream the horizontal normal stress decreases at a slower rate. The increased horizontal normal stress may be explained by increased turbulent production due to the velocity gradient being greater for the narrower jet observed in the stratified case.

The vertical normal stress measurements (Fig. 6) for the unstratified jet are slightly lower than the semi-empirical curve, but the decay rate is similar. The stratified case demonstrates very different behavior. The vertical normal stress is substantially smaller compared to the unstratified case for  $x/D < 80$  ( $x/l_N < 2.9$ ). Beyond  $x/D = 80$ , the vertical normal stress approaches and then exceeds the unstratified case. In contrast to these data, it is usually assumed that the vertical fluctuations are most significantly affected beyond the collapse location. The increased vertical normal stress for large  $x/D$  also may be explained by the increased mean velocity gradient in the narrower stratified jet.

The flow visualization images indicate a clear transition at  $x/D = 80$  ( $x/l_N = 2.9$ ), while the centerline velocity measurements fail to reveal a distinct transition. At this location the Ozmidov scale is  $L_R = (\varepsilon/N^3)^{1/2} \approx 0.09$  m, where  $\varepsilon$  was estimated from the measured velocity fluctuations and vertical jet half-width. The vertical jet width is 0.06 m at this location; thus, this location agrees very well with Gibson's (1987) transition criteria,  $L_R \approx (1.5 \pm 0.5)w$ . The measurements also agree very well with Ivey and Imberger's (1991) transition criterion,  $Fr_T \approx 1$ , assuming the overturn length scale equals the jet width. [It should be noted that Roberts and Matthews (1987) found a minimum value of 0.75 in a turbulent jet by assuming the important length scale is the longest scale.] In addition, the dimen-

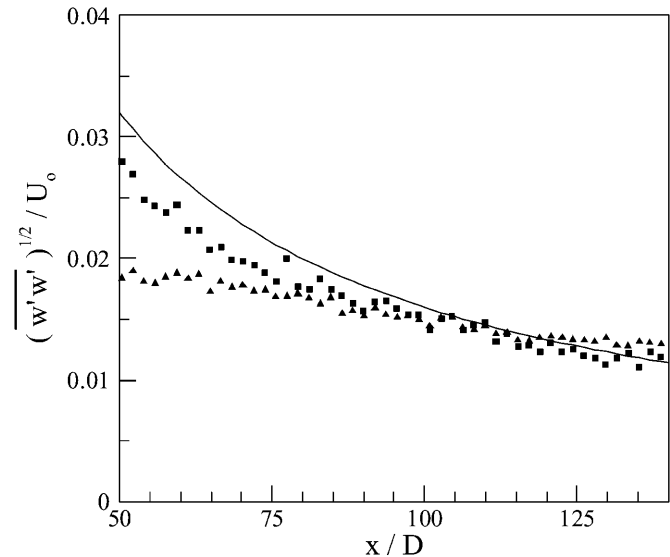


Fig. 6. Vertical normal stress for the unstratified (■) and stratified (▲) jets. The curve is the semi-empirical expression  $(\overline{w'w'})^{1/2}/U_o = 1.5D/x$

sionless shear number,  $S^*$ , increases to a value of approximately 7.5 at  $x/D = 80$  and then remains constant downstream. Approaching a constant value is consistent with in the DNS simulations of Shih et al. (2000), although the value is slight smaller than their observation for homogeneous sheared turbulence.

Six mean velocity profiles are shown in Fig. 7 for the unstratified case. By non-dimensionalizing with the mean centerline velocity and distance from the nozzle, the data collapses onto a single curve, indicating self-similar behavior. Also shown in Fig. 7 is the Gaussian curve reported by Fischer et al. (1979) and others. The half-width of the jet,  $b_u = 0.120x$ , is within the range reported by Fischer et al. (1979) (i.e., the constant is between 0.97 and 0.130).

Corresponding profiles for the stratified case are shown in Fig. 8. The locations correspond to  $x/l_N = 2.1$  (●), 2.7 (■), 3.3 (▲), 3.9 (▼), 4.5 (►), 5.1 (◆). Although the differences are subtle, the profiles do not collapse on a single self-similar curve. The profiles become gradually narrower with distance from the nozzle, which is consistent with the suppressed vertical expansion seen in the flow visualization images.

The six profiles of the vertical normal stress shown in Fig. 9 for the unstratified jet collapse fairly well onto a single behavior. The magnitude is slightly higher than the hot-wire anemometry measurements of Wgnanski and Fiedler (1969), although they agree well with the measurements of Webster et al. (2001). In contrast, a clear trend is observed in the vertical normal stress profiles for the stratified case. Shown in Fig. 10, the six profiles can be clearly discriminated from each other. The values are generally lower than those observed in the unstratified jet, indicating the vertical fluctuations are suppressed by the stratification. In addition, the normalized vertical normal stress increases with distance from the nozzle. This indicates that the centerline velocity decays faster than the

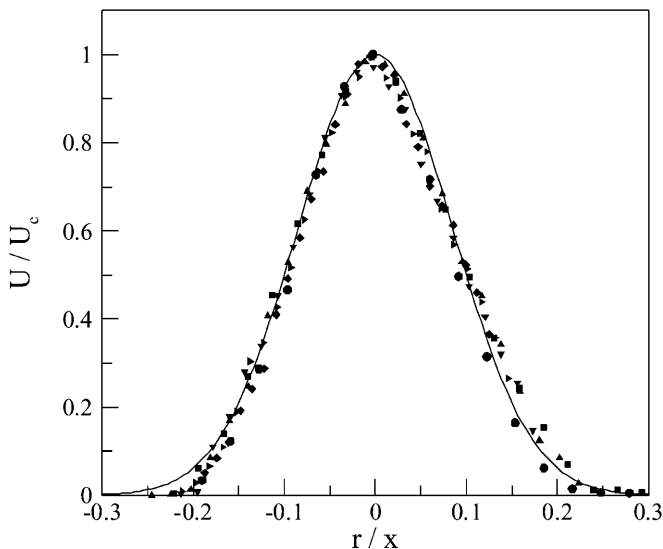


Fig. 7. Self-similar mean velocity profiles for the unstratified jet. The curve is the empirical expression:  $U/U_c = \exp\{-(r/0.120x)^2\}$ .  $x/D = 58$  (●), 74 (■), 90 (▲), 106 (▼), 122 (►), 138 (◆)

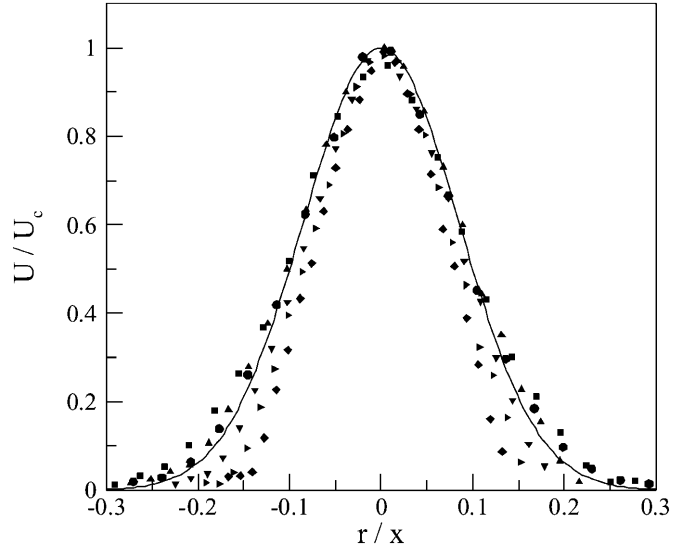


Fig. 8. Velocity profiles for the stratified jet. The curve is the empirical expression for the unstratified jet:  $U/U_c = \exp\{-(r/0.120x)^2\}$ . Symbols are the same as Fig. 7

vertical fluctuations, which is consistent with the profiles shown in Figs. 4 and 6.

Profiles of horizontal normal stress are not shown here. However, both the unstratified and stratified cases appear to collapse onto a single curve and the profiles agree very well with the measurements of Wgnanski and Fiedler (1969). Although  $\overline{u'u'}$  is larger along the centerline in the stratified jet case (Fig. 5), its normalizing scale  $U_c$  is also larger. The centerline mean velocity decreases at the same rate as the horizontal normal stress, thus the normalized profiles collapse onto a single behavior.

The shear stress profiles shown in Fig. 11 for the unstratified jet agree with Wgnanski and Fiedler (1969) and demonstrate the expected self-similarity. In the stratified jet case (Fig. 12), the magnitude of the shear stress is roughly a

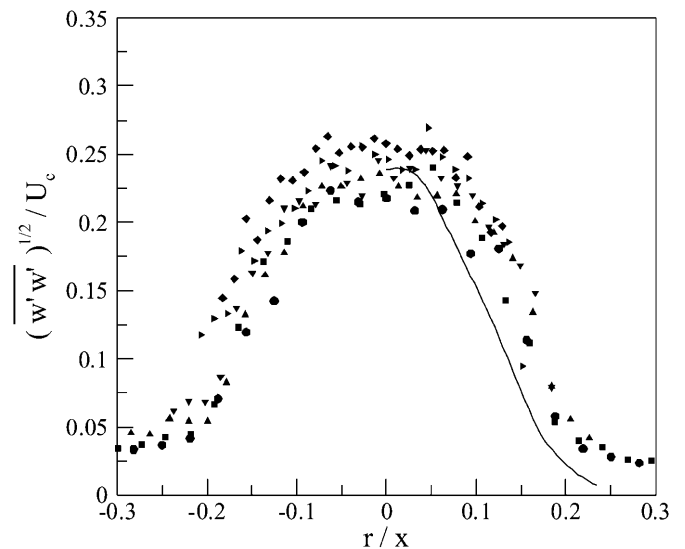


Fig. 9. Self-similar profiles of the vertical normal stress for the unstratified jet. The curve is data from Wgnanski and Fiedler (1969). Symbols are the same as Fig. 7

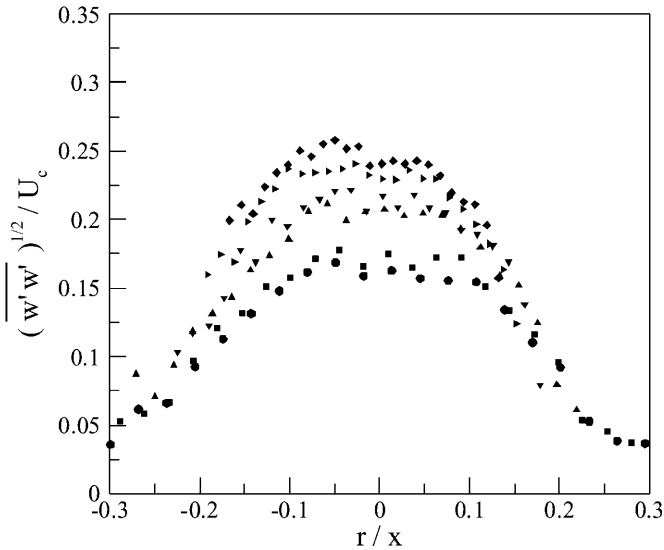


Fig. 10. Profiles of the vertical normal stress for the stratified jet. Symbols are the same as Fig. 7

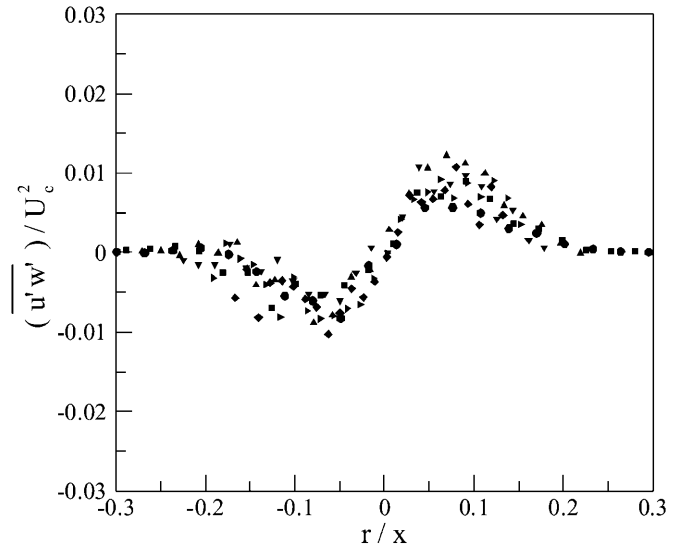


Fig. 12. Profiles of the shear stress for the stratified jet. Symbols are the same as Fig. 7

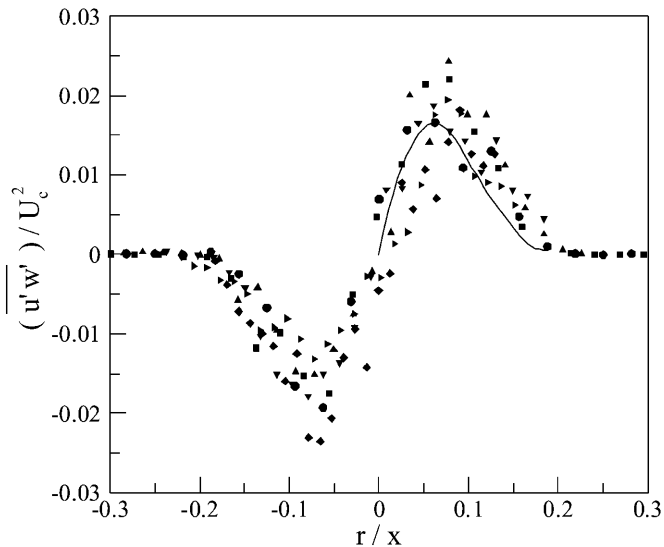


Fig. 11. Self-similar profiles of the shear stress for the unstratified jet. The curve is from Wygnanski and Fiedler (1969). Symbols are the same as Fig. 7

factor of two smaller than the unstratified case and the profiles collapse onto the same curve. Since the flow visualization images indicate that the jet expansion in the vertical direction is suppressed beyond  $x/l_N = 2.9$ , it would be expected that the shear stress, which is largely responsible for the momentum transport across the shear layer and hence the expansion of the jet, would be diminished. While the magnitude of the shear stress is indeed reduced, the lack of an obvious transition indicates that transport is suppressed over the entire measurement region.

#### 4

#### Conclusion

The turbulent velocity characteristics of horizontal jets in unstratified and stratified fluid environments have been

studied. Estimates of the turbulence collapse location from flow visualization images agree well with previous observations. Velocity field measurements of the unstratified jet agree well with previous point measurements, thus demonstrating the effectiveness of the DPTV measurement technique. The velocity fields demonstrate a strong influence of the density stratification. Normalized plots of centerline mean velocity and turbulent normal stresses differ from the semi-empirical curve for the unstratified case. The results indicate that the vertical fluctuations are indeed attenuated, but surprisingly the attenuation appears greatest closer to the nozzle than  $x/l_N = 2.9$ , the collapse location inferred from the flow visualization images. Finally, the turbulent shear stress, which is the dominant mechanism for transport of momentum across the shear layer, is greatly reduced over the entire measurement region compared to the unstratified case.

#### References

- Boyer DL; Davies PA; Fernando HJS; Zhang X (1989) Linearly stratified flow past a horizontal circular cylinder. *Phil Trans R Soc Lond Ser A* 358: 501–528
- Cowen EA; Monismith SG (1997) A hybrid digital particle-tracking velocimetry technique. *Exp Fluids* 22: 199–211
- Davero G; Roberts PJW; Maile K (2001) Refractive index matching in large-scale stratified experiments. *Exp Fluids* 31: 119–126
- Fischer HB; List EJ; Koh RCY; Imberger J; Brooks NH (1979) *Mixing in inland and coastal waters*. Academic Press, New York
- Fortuin JMH (1960) Theory and application of two supplementary methods of constructing density gradient columns. *J Polym Sci* 44: 505–515
- Gibson CH (1980) Fossil temperature, salinity, and vorticity turbulence in the ocean. In: Nihoul J (ed) *Marine Turbulence*. Elsevier Science, Amsterdam, pp 221–257
- Gibson CH (1987) Fossil turbulence and intermittency in sampling oceanic mixing processes. *J Geophys Res* 92: 5383–5404
- Gibson CH (1990) Turbulence, mixing and microstructure. In: Le Mehande B, Hanes DM (eds) *The Sea*. Ocean Engineering Science, vol. 9, part A. Wiley-Interscience, New York, pp 631–659

- Hannoun IA; Fernando HJS; List EJ** (1988) Turbulence structure near a sharp density interface. *J Fluid Mech* 189: 189–200
- Holt SE; Koseff JR; Ferziger JH** (1992) A numerical study of the evolution and structure of homogeneous stably stratified sheared turbulence. *J Fluid Mech* 237: 499–539
- Ivey GN; Imberger J** (1991) On the nature of turbulence in a stratified fluid. Part I. The energetics of mixing. *J Phys Oceanogr* 21: 650–658
- Jacobitz FG; Sarkar S; Atta CW Van** (1997) Direct numerical simulations of the turbulence evolution in a uniformly sheared and stably stratified flow. *J Fluid Mech* 342: 231–261
- List EJ** (1971) Laminar momentum jets in a stratified fluid. *J Fluid Mech* 45: 561–574
- Piccirillo PS; Van Atta CW** (1997) The evolution of a uniformly sheared thermally stratified turbulent flow. *J Fluid Mech* 334: 61–86
- Roberts PJW; Matthews PR** (1984) Dynamics of jets in two-layer stratified fluids. *J Hydraul Eng* 110: 1201–1217
- Roberts PJW; Matthews PR** (1987) Behavior of low-buoyancy jets in a linearly stratified fluid. *J Hydraul Res* 25: 503–519
- Roberts PJW; Maile K; Daviero G** (2001) Mixing in stratified jets. *J Hydraul Eng* 127: 194–200
- Rohr JJ; Itsweire EC; Helland KN; Van Atta CW** (1988) Growth and decay of turbulence in a stably stratified shear flow. *J Fluid Mech* 195: 77–111
- Shih LH; Koseff JR; Ferziger JH; Rehman CR** (2000) Scaling and parameterization of stratified homogeneous turbulent shear flow. *J Fluid Mech* 412: 1–20
- Voropayev SI; Afanasyev YD** (1991) Steady horizontal jet in a stratified fluid. *Mech Res Comm* 18: 435–440
- Webster DR; Roberts PJW; Ra'ad L** (2001) Simultaneous DPTV/PLIF measurements of a turbulent jet. *Exp Fluids* 30: 65–72
- Wyganski I; Fiedler H** (1969) Some measurements in the self-preserving jet. *J Fluid Mech* 38: 577–612
- Xu Y; Fernando HJS; Boyer DL** (1995) Turbulent wakes of stratified flow past a cylinder. *Phys Fluids* 7: 2243–2255